Journal of Power Sources 196 (2011) 1808–1817

Contents lists available at ScienceDirect

Journal of Power Sources

journal homepage: www.elsevier.com/locate/jpowsour

The electrical properties of microwave sintered gadolinia doped ceria–alumina nano-composite electrolyte

Rajalekshmi Chockalingam, Sreekumar Chockalingam*, Vasantha R.W. Amarakoon

New York State College of Ceramics at Alfred University, Alfred, NY, USA

ARTICLE INFO

Article history:
Received 7 September 2010
Accepted 21 September 2010
Available online 1 October 2010

Keywords:
Chemical synthesis
Ceria–alumina nano-composite
Microwave sintering
Impedance spectroscopy
Electrical conductivity
Solid oxide fuel cells

ABSTRACT

Gadolinia doped ceria–alumina (GDC–Al_2O_3) nano composites have been prepared by chemical synthesis route and sintered using 2.45 GHz microwave energy as well as conventional technique. The electrical properties of the sintered samples are investigated by ac impedance spectroscopy. It has been observed that the conductivity of microwave sintered GDC–Al_2O_3 composite is higher than that of conventional sintered GDC–Al_2O_3 composite and pure GDC sample. Higher concentration of vacancies at the interfaces of GDC and Al_2O_3 phases may be responsible for the better conductivity of GDC–Al_2O_3 composite compared to pure GDC. The fine grain microstructure of microwave sintered samples creates more interfaces compared to conventional sintered sample which in turn responsible for the better performance of microwave sintered composite sample. The micro-structural results of microwave sintered samples also reveal the presence of elongated, needle like Al_2O_3 grains. The X-ray diffraction results have shown the formation of additional $GdAlO_3$ phase.

1. Introduction

State of the art yttria stabilized zirconia (YSZ) based solid oxide fuel cells (SOFCs) require expensive sealing and interface materials due to their high operating temperature in the range of 800–1000 °C [1]. Doped ceria has been extensively investigated as an alternative solid electrolyte capable of operating at intermediate-temperature in the range of 500–700 °C. Ceria based SOFCs also exhibit higher ionic-conductivity than that of ZrO_2 [2]. However, at lower oxygen partial pressures (below 10^{-6}) Ce^{4+} reduces to Ce^{3+} leading to electronic conduction in addition to the oxygen ion conduction [3]. The resulting electronic conduction through the electrolyte reduces the open circuit voltage [4]. Mishima et al. [5] demonstrated that electronic conduction of samaria doped ceria at lower partial pressure could be reduced by adding Y_2O_3 stabilized ZrO_2. There were also reports suggesting that the addition of insulating second phase reduces the electronic conductivity of doped ceria by trapping electrons within space charge regions at the interface between the ceria and insulating grains [6]. Lee et al. [7] investigated the effect of Al_2O_3 addition on the sintering behavior of Gd doped CeO_2 and observed additional phase formation such as $AlGdO_3$ when more than 5 mol% Al_2O_3 is added to Gd doped CeO_2 and sintered above 1400 °C. Moreover, the formation of $AlGdO_3$ phase reduces the Gd content in CeO_2 matrix which in turn negatively affects the ionic conductivity of CeO_2–Al_2O_3 composite [8].

Recently sintering of ceramics using microwave energy received much attention due to its advantages over conventional sintering techniques such as lower sintering temperature, reduced sintering time, volumetric heating and capabilities of producing unique microstructure that could not otherwise possible to achieve by conventional methods [9–18]. Janney et al. [19] demonstrated that 8 mol% yttria stabilized zirconia for solid oxide fuel cell applications could be sintered to full density using 2.45 GHz microwaves 150 °C lower than conventional sintering techniques. The purpose of this work was to synthesise Gd–CeO_2–Al_2O_3 nano composites through chemical synthesis route and sinter at a lower temperature (below 1400 °C) using 2.45 GHz microwave energy and investigate the densification behavior, grain morphologies and electrical conductivity. The results of microwave sintered samples were compared with those of conventionally sintered samples.

2. Experimental procedures

2.1. Synthesis and sintering of CeO_2–Al_2O_3 nano-composites

The experimental procedure for the preparation of Gd doped CeO_2–Al_2O_3 nano-composite is shown in Fig. 1. Alumina sols were prepared by mixing 12 g of reagent grade $Al(OC_4H_9)_3$ (Sigma–Aldrich, Milwaukee, WI 53201, USA) with 900 g distilled water at 75 °C under vigorous stirring for 30 min. About 0.1 mol of

* Corresponding author at: National Physical Laboratory, Electronic Materials, Dr. K.S. Krishanan Marg, New Delhi, New Delhi 110012, India.
Tel.: +91 9910801320; fax: +91 11 45609320.
E-mail address: sreekumarchockalingam@gmail.com (S. Chockalingam).

0378-7753/$ – see front matter © 2010 Elsevier B.V. All rights reserved.
doi:10.1016/j.jpowsour.2010.09.074

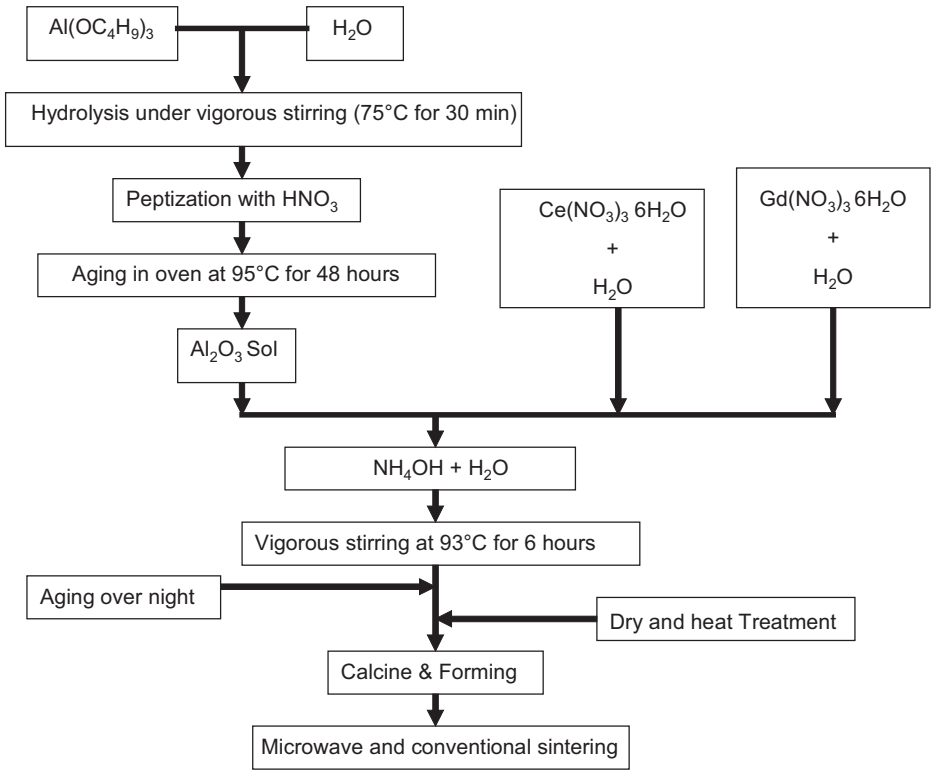

Fig. 1. Flowchart shows the procedure for the preparation of Gd–CeO_2–Al_2O_3 nano composite powder.

concentrated HNO_3 (Sigma–Aldrich, Milwaukee, WI 53201, USA) was added to the solution and aged for 48 h at 95 °C. The 0.1 mol of concentrated HNO_3 was intentionally selected to form both circular and elongated alumina particles. A white colored suspension was formed. The suspension was kept for a week at room temperature and no precipitate was formed and the particles never settled down. The freshly prepared 125 g of alumina sol, 20.74 g of $Ce(NO_3)_2{\cdot}6H_2O$ (Sigma–Aldrich, Milwaukee, WI 53201, USA) and 5.388 g of $Gd(NO_3)_2{\cdot}6H_2O$ (Sigma–Aldrich, Milwaukee, WI 53201, USA) were then added together to 700 ml of distilled water. Ammonia solution was slowly added and continued stirring for 6 h at 93 °C followed by additional 12 h aging. After evaporating the water at 100 °C, heat treatment was performed at 900 °C for 4 h in air. The heat treated powders were ground and sieved through a 38 μm mesh. Three grams of the powders were die-pressed at 30 MPa and cold isostatically pressed at 200 MPa into cylindrical green pellets of diameter 11 mm and thickness of 3 mm. Conventional sintering of the samples was performed in an alumina tube furnace. Microwave sintering trials were performed in a 2200 W laboratory model microwave furnace. The temperature of the samples was measured with the help of calibrated type C thermocouple. Fig. 2 shows the refractory setup used for microwave sintering. It consists of 2.45 GHz microwave transparent alumina fiber board insulation and small pieces of SiC microwave susceptors for preheating the samples, Fig. 3 compares the heating profiles used for microwave and conventional sintering of Gd–CeO_2–Al_2O_3. The heating rate was 5 °C min^{-1} in the case of microwave sintering and 2 °C min^{-1} for conventional sintering.

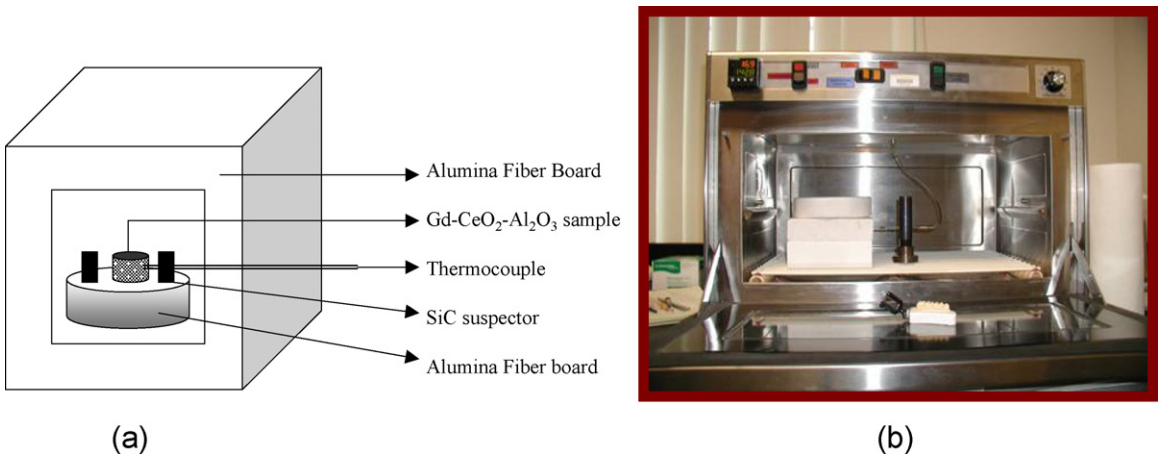

Fig. 2. Alumina refractory with temperature measurement setup used for microwave sintering (a) and original photograph showing high temperature laboratory microwave furnace with sintering setup (b).

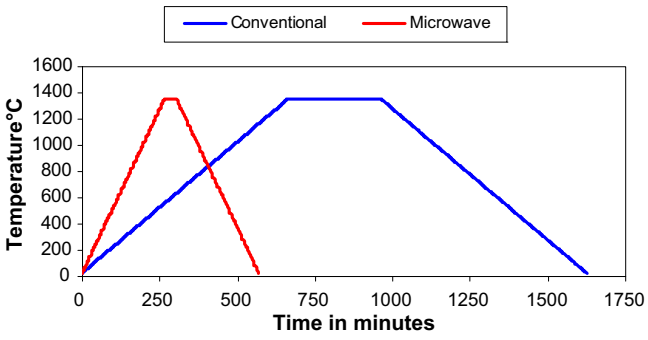

Fig. 3. Comparison of microwave and conventional sintering cycles to sinter Gd–CeO_2–Al_2O_3 composites.

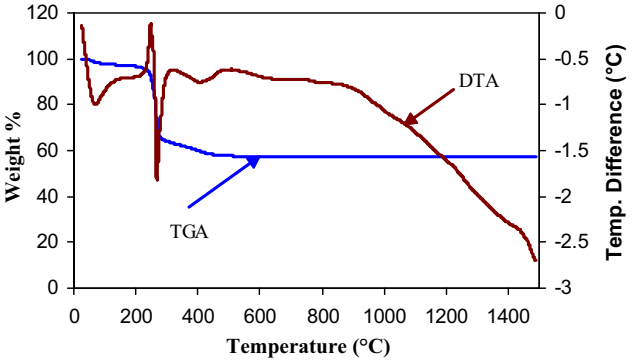

Fig. 4. TGA and DTA analysis of Gd–CeO_2–Al_2O_3 nano composite powder.

2.2. Characterization of CeO_2–Al_2O_3 nano-composites

The microstructures of the powder as well as sintered samples were evaluated using a Hitachi HF2000 Field Emission Transmission Electron microscopy (TEM) and energy dispersive X-ray spectroscopy (EDS). TEM specimens were prepared from pellets along cross-sectional direction. Phase analysis of the prepared powder and sintered samples was carried by X-ray diffraction (Philips, XRG 3100 X-ray generator). The prepared powders were heat treated for 2 h at (a) 300 °C, (b) 500 °C, (c) 700 °C, (d) 900 °C and continued for 4 h and 6 h at 900 °C. The generator was set to 40 kV and 20 mA utilizing Cu-Kα radiation. X-ray diffraction pattern was analyzed using a software package JADE 7 (Materials Data, Livermore, CA). Differential thermal analysis (DTA) and thermo gravimetric analysis (TGA) were performed using SDT 2960 simultaneous DSC–TGA. The experiments were performed in air up to 1500 °C with a heating rate of 10 °C min^{-1}. The data acquisition and processing were carried out using the software Universal Analysis 2000. Densities of the samples were determined using Archimedes principle with de-ionized water.

AC impedance measurements were carried out in a Solartron1260 impedance/gain analyzer along with a Centurion Qex furnace. The samples were placed in between two platinum electrodes connected to the impedance analyzer. Data were collected with the help of Labview software (Version 6, National Instruments, 2000) at 100 °C intervals from room temperature using a frequency range of 1 Hz to 10 MHz. Nyquist plots were then generated at each temperature interval and analyzed in the Z-View software (Version 2.6 Scribner Associates Inc., Southern Pines, NC, 2002). The conductivity in S cm^{-1} was then determined for each composition.

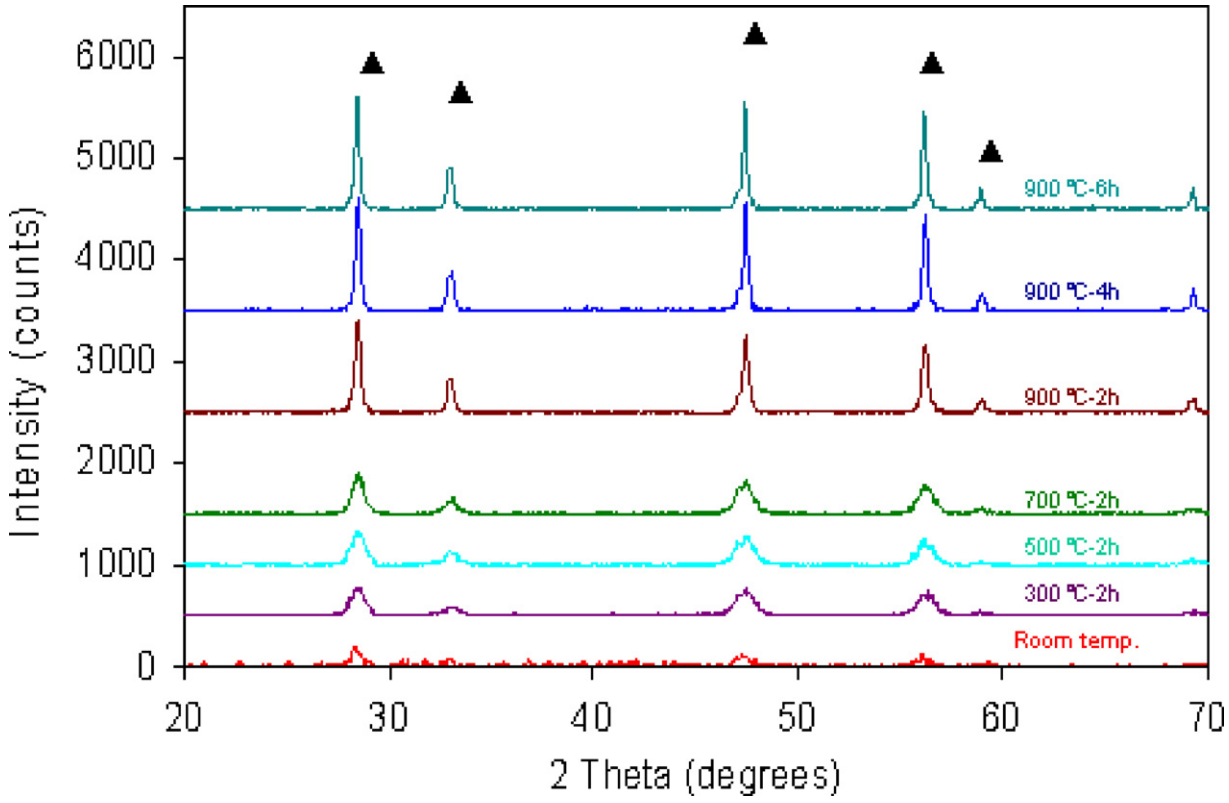

Fig. 5. Series of room temperature XRD patterns of Gd–CeO_2–Al_2O_3 powder heat treated at various temperatures starting from room temperature through 900 °C (● represents $Gd_{0.20}Ce_{0.80}O_{1.90}$ matches with PDF card 01-075-0162).

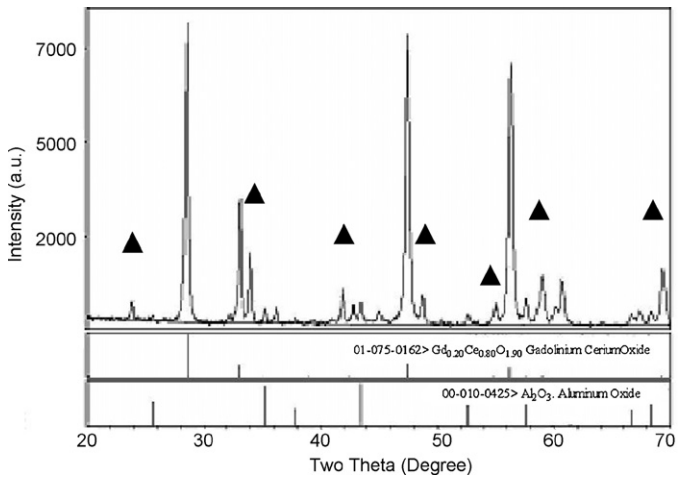

Fig. 6. XRD patterns of conventional sintered Gd–CeO_2–Al_2O_3 nano composite at 1450 °C for 300 min. The symbol ▲ represents $GdAlO_3$ [8].

3. Results and discussion

3.1. Characterization of the starting material

Fig. 4 shows typical thermal curves (TGA–DTA) of Gd–CeO_2–Al_2O_3 nano-composite powder. The first weight loss from room temperature to 200 °C is associated with an endothermic peak ~70 °C in the DTA curve caused by the loss of molecular water. One can also observe a second weight loss from 200 °C to 300 °C as well as an exothermic peak at ~220 °C and an endothermic peak at ~250 °C. The exothermic peak at 200 °C may be most likely caused by the oxidation of cerium based hydrate [20] and/or re-crystallization of hydrate. The endothermic peak at 250 °C may be due to the decomposition of cerium based hydrate [20]. Finally, the third weight loss from 300 °C to 450 °C coupled with an endothermic peak at 400 °C may be due to the loss of organic residues [21]. X-ray diffraction was performed to study the crystalline nature and phase purity of prepared Gd doped CeO_2–Al_2O_3 nano-composite powders. Characteristic diffraction peaks corresponding to fluorite like structure were formed around 2 h of heat treatment of the powders at 300 °C (Fig. 5). The broad peaks suggest the presence of small particle sizes. The sharp peaks at 900 °C indicate that as the heat treatment temperature increases the particle size also increases. XRD patterns never revealed any secondary phases indicating that alumina remains amorphous state up to 6 h of heat treatment at 900 °C.

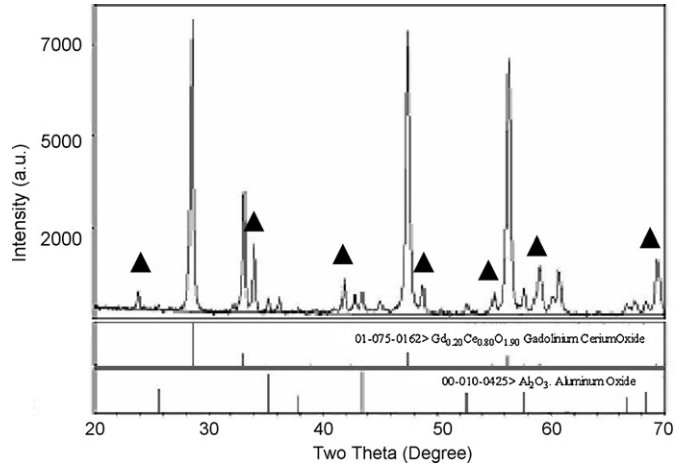

Fig. 7. XRD patterns of microwave sintered Gd–CeO_2–Al_2O_3 nano composite at 1350 °C for 40 min. The symbol ▲ represents $GdAlO_3$ [8].

3.2. Densification behavior of CeO_2–Al_2O_3 nano-composites

The density of microwave sintered sample at 1350 °C for 40 min is 5.20 g cm^{-3}, and conventional sintered sample is 4.13 g cm^{-3} at similar temperature and hold time. However, the conventional sintered sample reached a density of 5.19 g cm^{-3} when sintering was performed at a higher temperature of 1450 °C for 300 min. The enhanced densification observed in the case of microwave sintered samples could be explained based on reverse thermal gradient, a well known phenomenon occurs due to volumetric heating

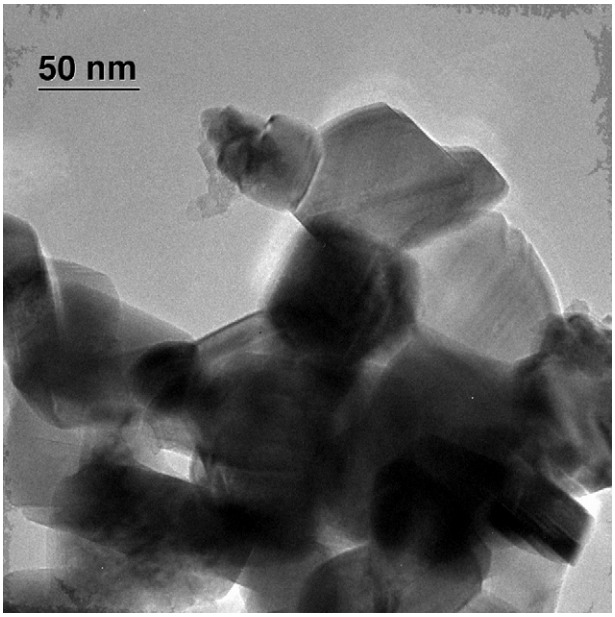

Fig. 8. Bright field (BF) transmission electron microscopy (TEM) image of the Gd–CeO_2–Al_2O_3 nano composite powder, showing the nano-particles.

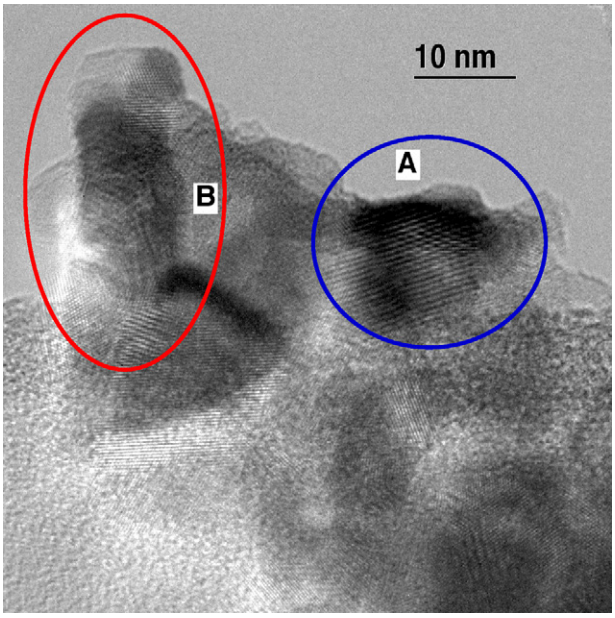

Fig. 9. The TEM image clearly shows the formation of Al_2O_3 nano-particles. The dimensions of grain-B is approximately 25 nm length and 10 nm width and the aspect ratio is 2.5. The diameter of grain-A is approximately 15 nm.

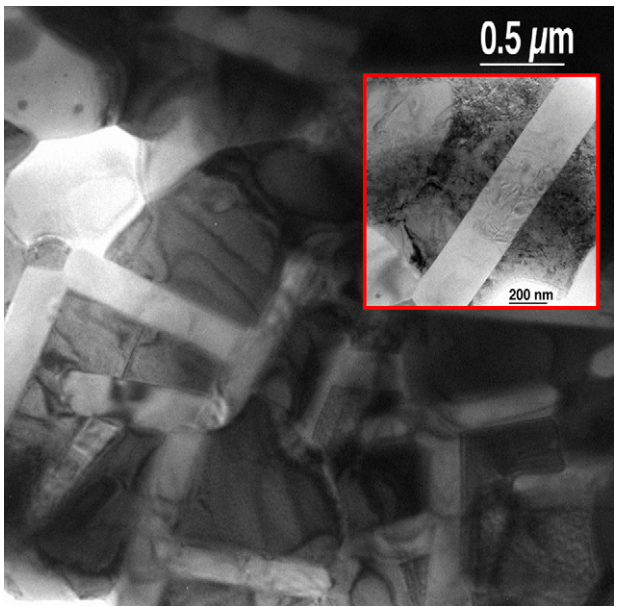

Fig. 10. BF-TEM image of microwave sintered Gd–CeO_2–Al_2O_3 nano-composite at 1350 °C showing elongated Al_2O_3 grains. The inset shows the high aspect ratio of one of the Al_2O_3 grains.

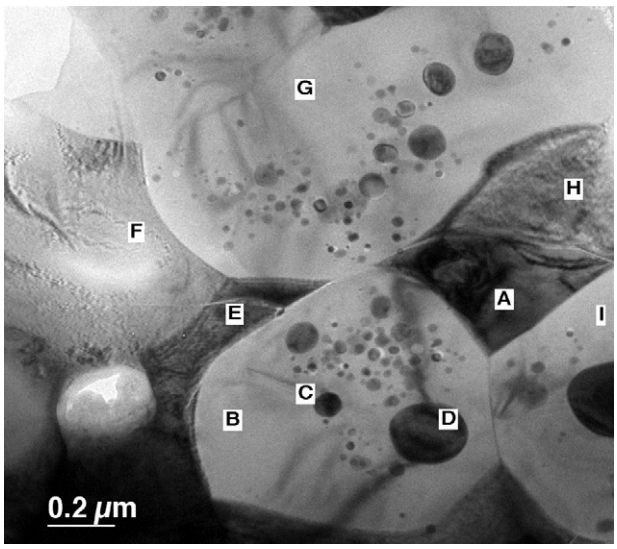

Fig. 11. BF-TEM image of Gd–CeO_2–Al_2O_3 nano-composite microwave sintered at 1350 °C showing the CeO_2 grains (labeled as A, E, F and H) and CeO_2 inclusions (labeled as C, D) within Al_2O_3 grain (labeled as B and G).

nature of microwaves. Center of the sample is at higher temperature than that of the surface. The difference in temperature causes reverse porosity gradient which in turn accelerate the densification to obtain a higher final density compared to conventionally sintered samples. One can also correlate the densification behavior to "microwave effect" a non-thermal driving force which partially compensate the thermal energy required to reduce the surface area of the powder particles [22–26]. As a result less thermal energy is required to initiate the sintering process by the use of microwave energy and densification of the green body could be achieved at a lower temperature.

3.3. Phase and microstructural analysis of sintered Gd–CeO_2–Al_2O_3 composites

XRD result of conventional sintered sample is shown in Fig. 6 and microwave sintered sample is shown in Fig. 7. Both patterns look almost identical. The major phase identified is $Gd_{0.2}Ce_{0.8}O_{1.9}$ and minor phases are Al_2O_3 and $GdAlO_3$. XRD analysis software

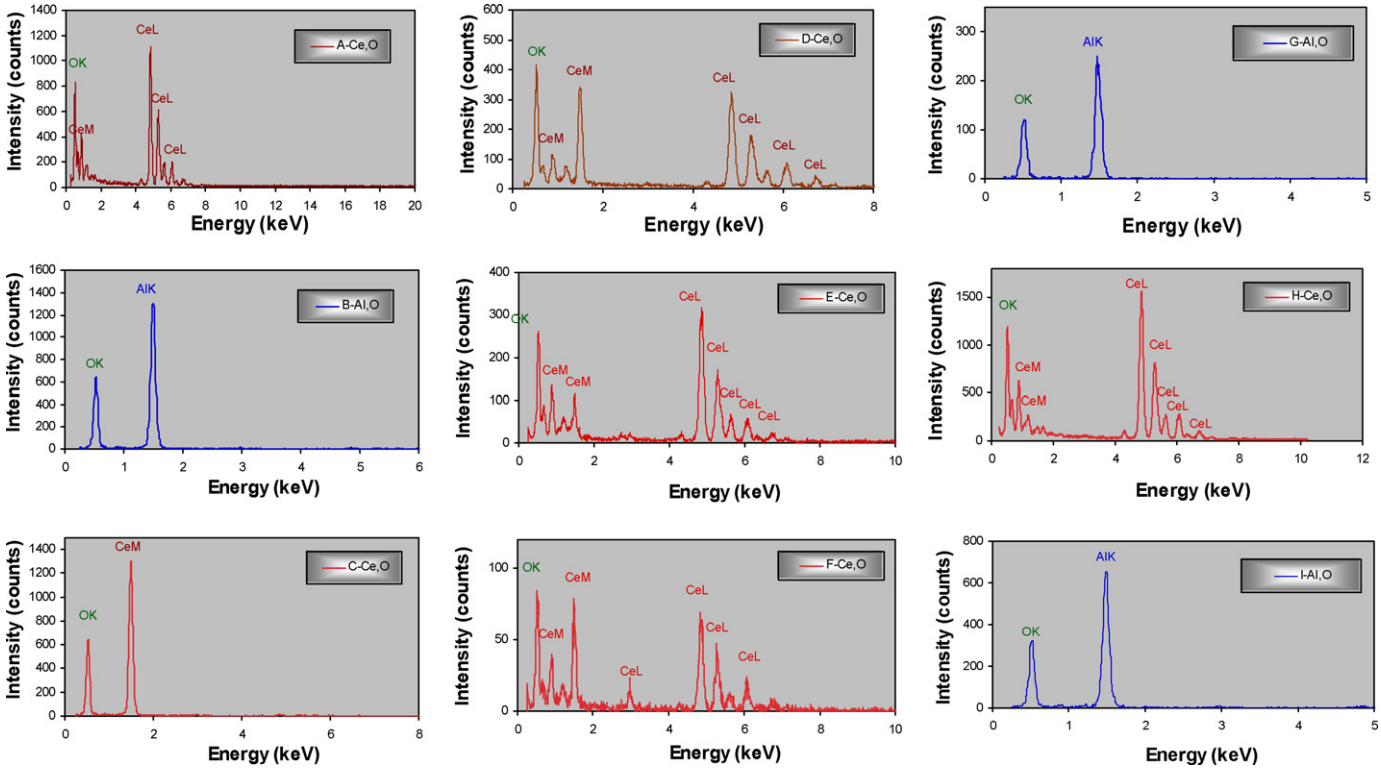

Fig. 12. EDS analysis of the microwave sintered Gd–CeO_2–Al_2O_3 nano-composite showing the details of chemical compositions. "A", "C", "D", "E", "F", "H" represent CeO_2, and "B", "G" and "I" represent Al_2O_3.

package JADE-7, did not identify the peaks corresponding $GdAlO_3$. Thus, the peaks representing $GdAlO_3$ were identified from the previous published work of Park and Choi [8] and Lee et al. [7]. In order to verify the formation of $GdAlO_3$, Lee et al. separately prepared $GdAlO_3$ by mixing aqueous solution of $Al(NO_3)_3{\cdot}9H_2O$ and $Gd(NO_3)_3{\cdot}6H_2O$ followed by sintering at 1400 °C. They also confirmed that $GdAlO_3$ phase forms at 1400 °C. Interestingly, in the present study the $GdAlO_3$ phase was detected at 1350 °C in the case of microwave sintered sample. This could be due to the error in temperature measurement in a microwave environment using thermocouple. The thermocouple was in contact with the sample and measuring the surface temperature of the sample which is obviously lower than the actual temperature at the center of the sample due to reverse thermal gradient caused by the volumetric nature of microwave heating [18]. The sample surface loses its heat by convection and radiation at higher temperatures. It is generally agreed that accurate measurement of the temperature during microwave processing is very challenging and neither thermocouple nor optical radiation pyrometer provides reliable reading [16].

Fig. 8 shows the bright field TEM image of the unagglomerated nano particles. Most of the particles were ~50 nm in diameter. The TEM image (Fig. 9) shows the formation of Al_2O_3 nano-particles with dimensions of approximately 25 nm length and 10 nm width (B) and 15 nm diameter (A). The formation of Al_2O_3 particles could be explained based on the acid/alkoxide ratio selected for the synthesis of Al_2O_3 nano particles. Yoldas [27] observed Al_2O_3 particle shape changed from round to acicular when the acid/alkoxide ratio (mol:mol) changed from 0.035 to 0.07. When the ratio increased from 0.07 to 0.14 the length increased from 50 nm to 100 nm. Based on the above argument, it is becoming clear that the acicular and rounded Al_2O_3 particles formed due to specific selection of acid/alkoxide ratio (0.1). During sintering process the acicular Al_2O_3 nano particles grown to become elongated Al_2O_3 grains as shown in TEM image (Fig. 10). Very recently, Zhang et al. [28] reported in situ growth of elongated Al_2O_3 grains when Al nano particles were added to α-Al_2O_3 powder. They also observed that the length of the alumina grains increased when the Al content increased from 0.01 to 0.1 wt%.

The inset of Fig. 10 shows the high aspect ratio of Al_2O_3 grain. The fiber like microstructure supports crack deflection and bridging; thus enhances the toughness of the composite structure [17]. Park and Choi reported [8] improvement in mechanical strength of Gd doped CeO_2 with the addition of small amounts of Al_2O_3. A typical bright-field (BF) TEM image of the microwave sintered sample at 1350 °C for 40 min is shown in Fig. 11 and the chemical composition of different phases is given in Fig. 12. The structure appears multi phase ceramic composite with Al_2O_3 and CeO_2 grains and CeO_2 particles of nanometer size are frequently trapped within the Al_2O_3 grains. The ceria rich phase present either as small inclusions within alumina grains or forms large grains. Fig. 13 displays a BF TEM image of the conventionally sintered sample at 1450 °C for 5 h with a heating rate of 2 °C min^{-1} and the chemical composition is given in Fig. 14. The phases identified were (i) Al_2O_3 rich phase with CeO_2 and Gd_2O_3 inclusions, (ii) CeO_2 and (iii) Gd_2O_3. Although Al_2O_3 grains appeared both elongated and rounded, mostly rounded grains were present. The diameter of the CeO_2 grains is less than one micrometer in diameter and the inclusions are less than 200 nm in size. The formation of fine CeO_2 inclusions within Al_2O_3 grains could be explained based on Heuer's argument [29]. The highly driven grain growth of 50 nm Al_2O_3 particles breakaway the grain boundaries and trap the CeO_2 particles. Further grain growth of the trapped CeO_2 particles is negligible due to the low lattice diffusivity of Al, Ce and O in Al_2O_3. Similar observations were previously reported in the literature [30,31].

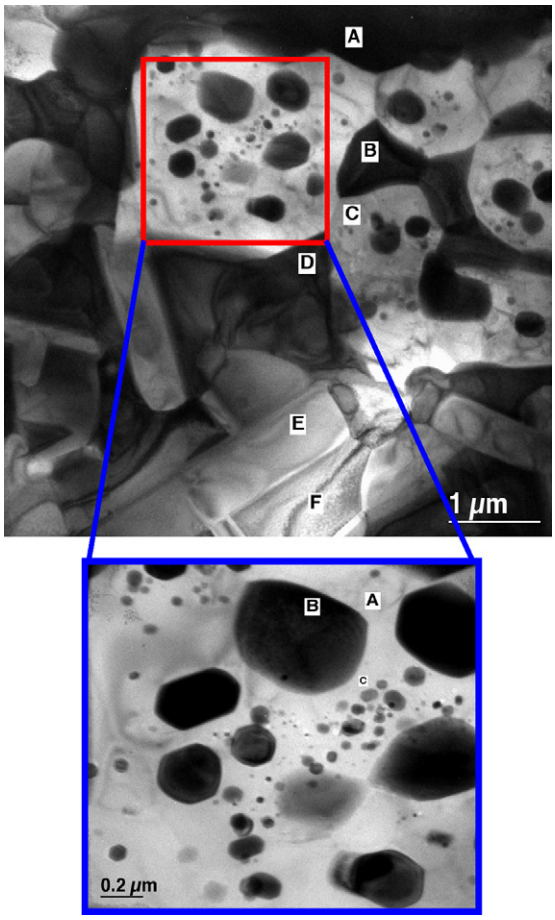

Fig. 13. BF-TEM image of conventionally sintered Gd–CeO_2–Al_2O_3 nano-composite at 1450 °C. The inset shows both CeO_2 (B) and Gd_2O_3 (C) inclusions within Al_2O_3 (A) grain.

The inset of Fig. 13 shows a single Al_2O_3 grain which clearly shows the CeO_2 and Gd_2O_3 inclusions. It is very interesting to see the presence of Gd_2O_3 (intra-granular) inclusions indicated as "C". This is not the case for the microwave sintered sample (Fig. 9), for which both intra and inter-granular Gd_2O_3 particles were completely absent. The diameter of CeO_2 grains was finer, of the order of 100 nm and rounded shaped compared to conventionally sintered sample which is about 500 nm in diameter and hexagonally shaped. The results indicate that the longer holding time of 300 min and slower heating rate of 2 °C min^{-1} of conventionally sintered sample was responsible for the excessive grain growth compared to microwave sintered sample, where the holding time was 40 min and heating rate was 5 °C min^{-1}. In general, sintering of consolidated powder particles takes place by the application of thermal energy. Such process is dependent on diffusion of atoms that combine powder particles into a grain. Sintering occurs well below the melting point of the material, but at a temperature high enough to allow an acceptable rate of diffusion of atoms through surface, grain boundary and grain to occur, usually greater than one-half of the melting-point of the material [32]. Surface diffusion of atoms requires less activation energy compared to grain boundary diffusion and occurs at lower temperature [33]. In the case of microwave sintering, one can argue that higher heating rate and volumetric nature of microwave heating could have been influenced the surface diffusion and suppressed the coarsening of grains that exist at lower temperatures resulting the development of a fine grain microstructure [33].

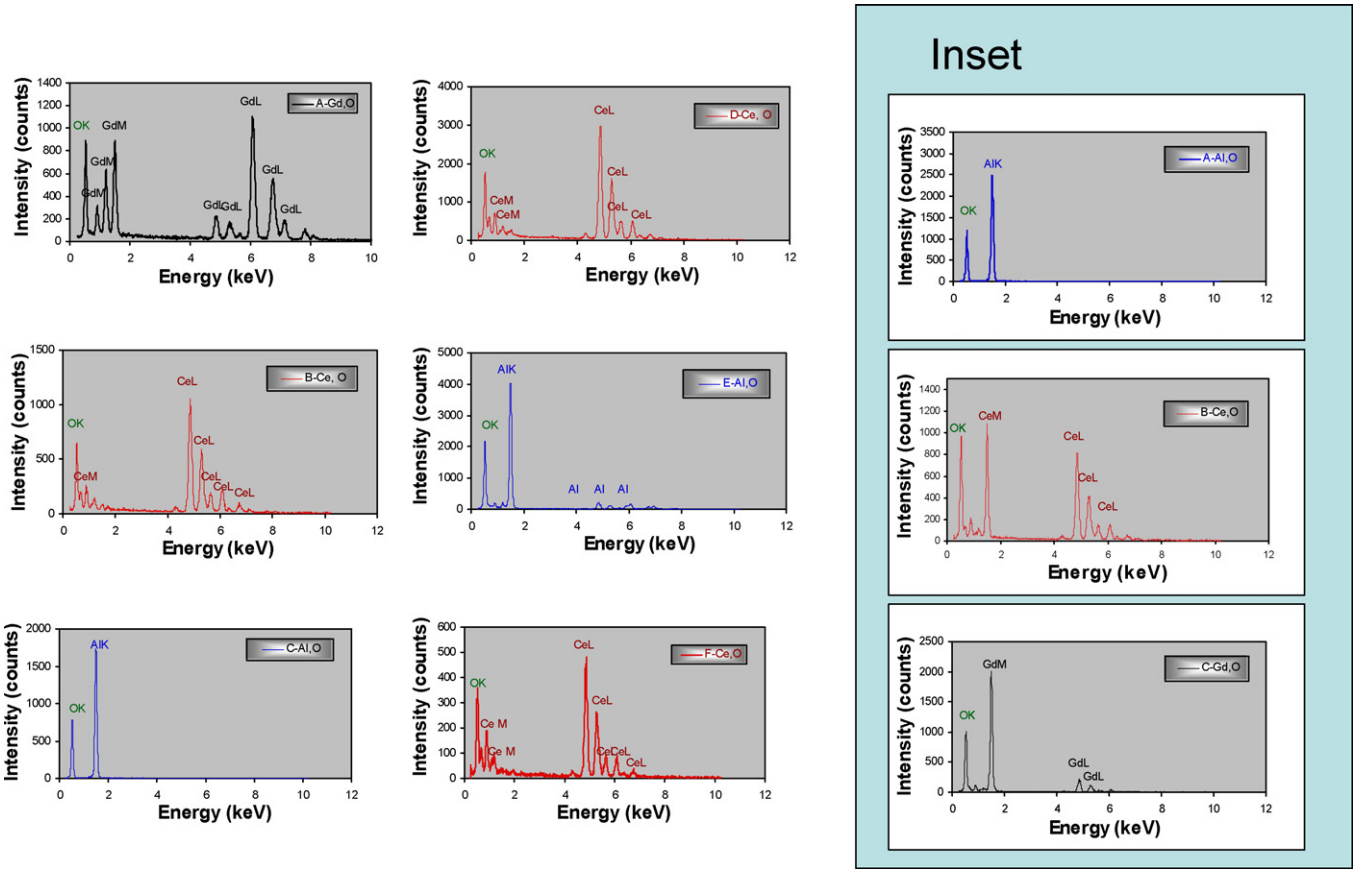

Fig. 14. EDS analysis of the conventionally sintered Gd–CeO_2–Al_2O_3 nano-composite showing the details of chemical compositions. "A" represents Gd_2O_3, "B", "D" and "F" represent CeO_2 and "C" and "E" represent Al_2O_3. In the inset "A" represents a single Al_2O_3 grain, "B" and "C" represent CeO_2 and Gd_2O_3 inclusions within Al_2O_3 grain.

3.4. Electrical conductivity

The conductivity of GDC–Al_2O_3 composite samples was measured by employing ac-impedance spectroscopy in air from 400 to 900 °C. The temperature of the sample is varied with the help of a split furnace. The experimental data obtained were fitted with electrical equivalent circuit model with parallel resistance and capacitance. The resulting Nyquist plot obtained was different from the ideal spectra of GDC, which consists of three distinct separate arcs representing grain (high frequency arc), grain boundary (intermediate frequency arc), and electrode (low frequency arc) whose time constant is sufficiently separated over the range of measurement frequencies [34]. The impedance plots of conventionally sintered GDC–Al_2O_3 sample in the selected temperatures range of 400–900 °C in air are presented in Fig. 15. The plots at 400 and 500 °C show only the responses from the bulk with rising electrode. The grain boundary arc is missing. This may be due to the increased relaxation frequency of grain boundary polarization [35]. When the measurement temperature was increased above 600 °C both the responses from the bulk and grain boundary appeared with electrode arc. It has been found that the total resistance of the sample decreases with increase in temperature. Fig. 16 shows the impedance spectra of microwave sintered GDC–Al_2O_3 sample. The total resistance of the sample found to be decreasing with increasing temperature. The spectrums at 400, 500 and 600 °C are quite similar to the conventional sintered samples, while the spectrums obtained above 600 °C look different. The grain boundary arcs are found to be depressed and the arcs which represent grains are incomplete, suggesting that the time constant of the grain response is too short. A common feature observed in the impedance spectra of both conventional and microwave sintered samples is the depressed grain boundary arc above 600 °C. The depressed grain boundary arc implies a constant phase element (CPE), originates from the inhomogeneities caused by variations in composition of grain boundary phase [35]. In the present investigation, one can probably argue that the depression of grain boundary arcs may be most likely due to the inhomogeneities caused by the interfaces between two phase regions such as GDC–Al_2O_3, GDC–Gd_2O_3 as evident in the TEM image (Fig. 17). However, it is important to note that presently no theory exist to support such an argument.

Fig. 18 compares the ionic conductivity of microwave and conventional sintered GDC–Al_2O_3 composites and pure GDC sample. The microwave sintered composite sample showed better conductivity compared to conventional sintered composite and pure GDC sample throughout the temperature range of interest. It is also interesting to note that GDC–Al_2O_3 composite samples showed better conductivity than that of pure GDC. Lee et al. [7] gave a plausible explanation for the increased conductivity observed in Al_2O_3 added GDC. They reported that within the solubility limit of Al_2O_3 in CeO_2 (2 mol%) Al^{3+} ions substitute Ce^{4+} ions.

The Kroger–Vink notation for such substitution can be written as [7].

$$Al_2O_3 \overset{CeO_2}{\rightleftarrows} 2Al'_{Ce} + 3O_O{}^{x} + V_O{}^{\bullet\bullet} \quad (1)$$

Oxygen vacancies are created to compensate the charge resulting enhanced oxygen ion conductivity. Similar results were also reported previously by Kang et al. [36]. They observed an increase of bulk conductivity in GDC when 5 mol% Al_2O_3 is added. Recently, Li et al. [37] reported a composite electrolyte made of doped lanthanum gallate and samarium doped ceria (LSGM–CSO) with better conductivity in the temperature range of 250–600 °C than that of single phase counterpart. They explained the observed high con-

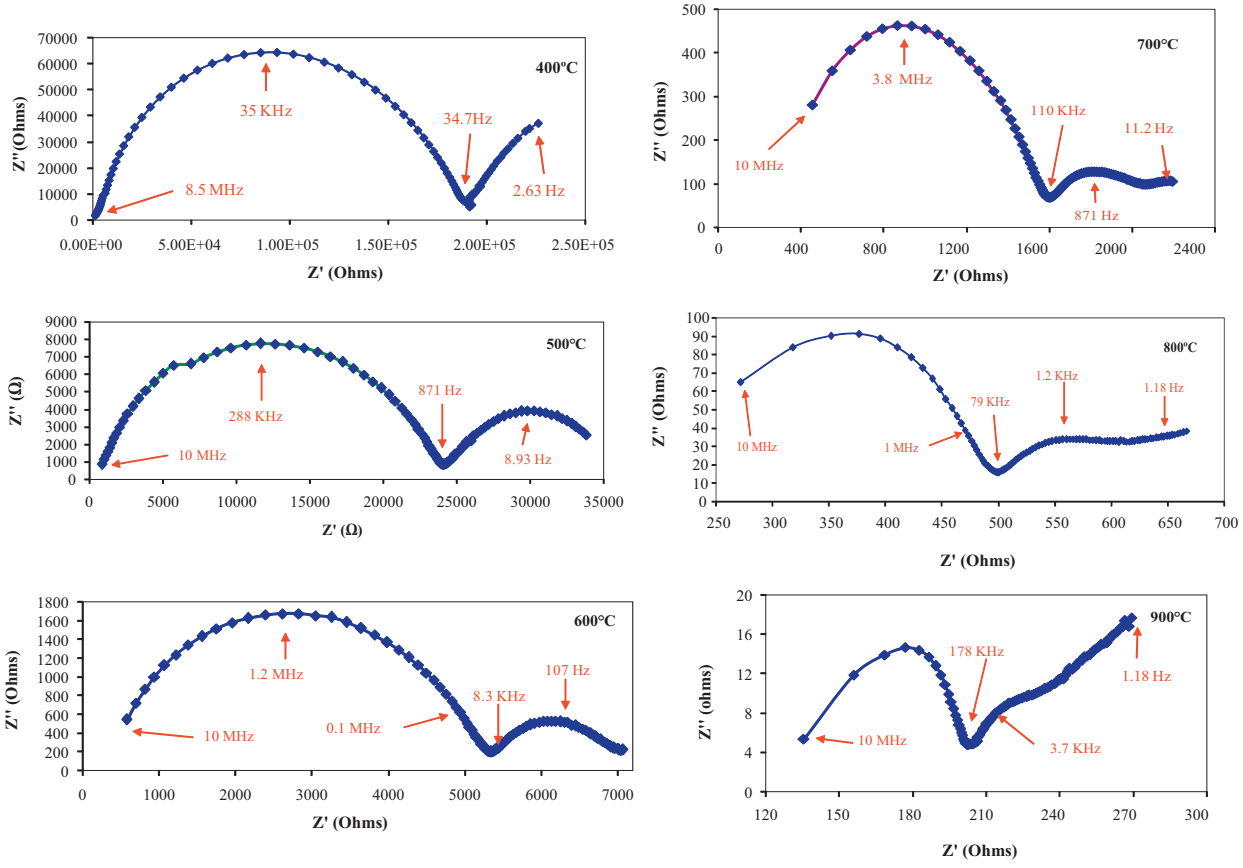

Fig. 15. The impedance plots of conventionally sintered GDC–Al_2O_3 sample in the selected temperatures range of 400–900 °C in air.

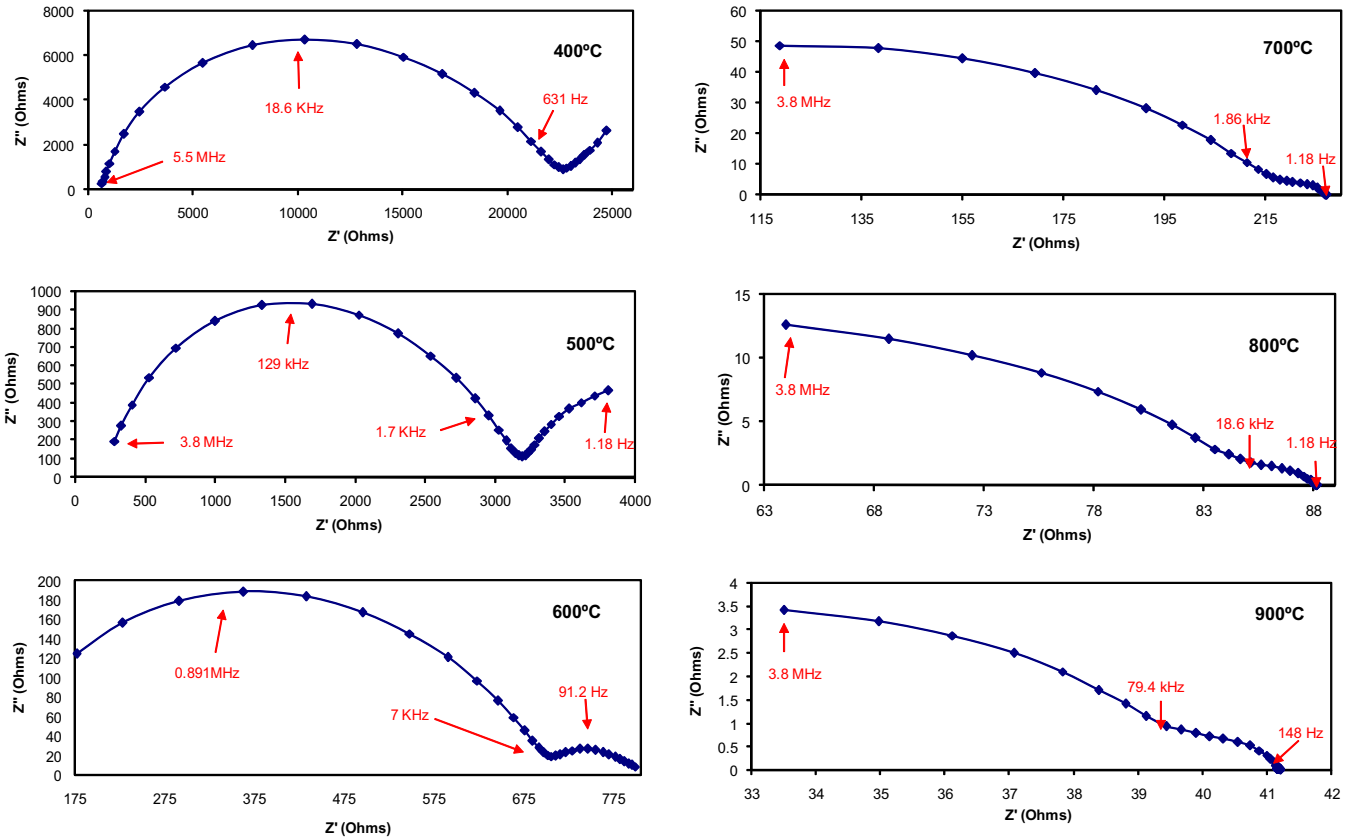

Fig. 16. The impedance plots of microwave sintered GDC–Al_2O_3 sample in the selected temperatures range of 400–900 °C in air.

Table 1
Activation energy for the sintered samples.

Sample specification	CON-GDC	MW-GDC–alumina	CON-GDC–alumina
Activation energy (eV) 300–600 °C	0.87	0.89	0.91
Activation energy (eV) 600–1000 °C	1.66	1.35	1.06

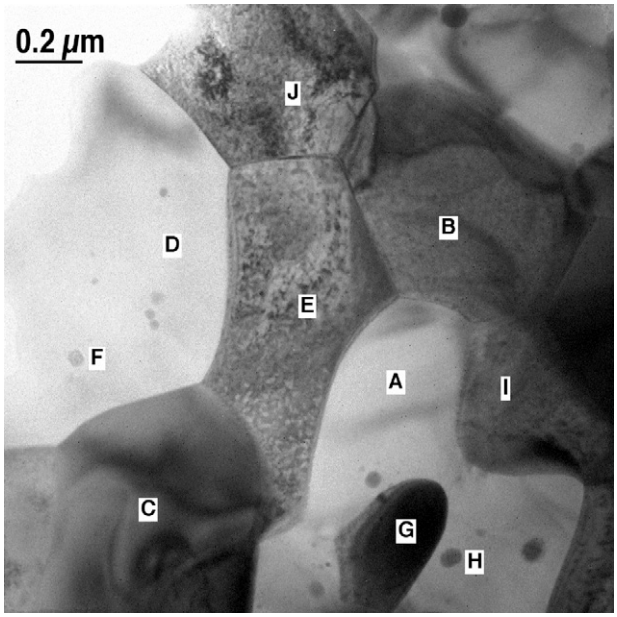

Fig. 17. BF-TEM image Gd–CeO_2–Al_2O_3 nano-composite microwave sintered at 1350 °C showing the CeO_2 grains (labeled as J, E, B and G), Al_2O_3 grain (labeled as F, D, A and H) and Gd_2O_3 grain (C).

ductivity of composite is due to the existence of space charge layer between the two phase regions. Based on the above collective arguments, one can suggest that the higher concentration of vacancies at the interfaces of GDC and Al_2O_3 phases is responsible for the better conductivity of GDC–Al_2O_3 composite compared to pure GDC. The fine grain microstructure of microwave sintered samples created more interfaces which in turn responsible for the better performance of microwave sintered composite sample. The activation energy for each case was calculated from the slopes of the linear fits in the Arrhenius plots and presented in Table 1. At lower temperature (300–600 °C) pure GDC showed lowest activation energy (0.87 eV) for oxygen ion migration, whereas at higher temperature (600–900 °C) conventional sintered GDC–Al_2O_3 composite showed lowest activation energy (1.06 eV). Maier [38] calculated the conductivity of a two-phase mixture of which one phase is an ionic conductor and the other phase is an insulator. The approach selected for solving the oxygen ion transport problem in heterogeneous media is a symmetrical, three-dimensional network of

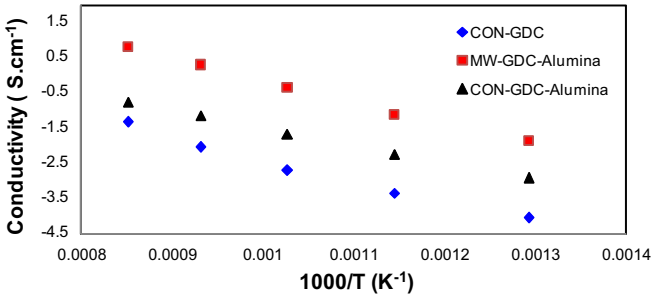

Fig. 18. Conductivity of microwave sintered GDC–Al_2O_3 and conventional sintered GDC–Al_2O_3 samples compared with pure GDC sample as a function of temperature.

percolating paths which taking into account the blocking effect. However, analysis of our results by applying Maier's model is out of the scope of this paper due to the complex topology of the distribution of various phases present in our system.

4. Conclusions

Gd–CeO_2–Al_2O_3 nano-composites have been synthesized through chemical route and densified using 2.45 GHz microwave energy at a lower temperature and dwell time compared to conventional sintering techniques. TEM microstructural analysis of sintered samples revealed frequent dispersion of CeO_2 particles within alumina grains. Al_2O_3 and Gd reacted during sintering and formed $GdAlO_3$ phase in both microwave and conventionally sintered samples. Microwave sintered GDC–Al_2O_3 composite samples exhibited fine grain microstructure and better conductivity than conventional sintered GDC–Al_2O_3 composite samples and pure GDC samples. Microwave sintering also favored the formation of isolated elongated Al_2O_3 grains with high aspect ratio which offers a possibility for improved fracture toughness of the composites.

Acknowledgement

The authors would like to gratefully acknowledge Dr. Jane Howe, High Temperature Materials Characterization Laboratory, ORNL for TEM analysis. Thanks are also due to Prof. Herbert Giesche and Prof. Doreen Edwards. CACT Center at Alfred University, NY is thankfully acknowledged for financial support.

References

[1] N.Q. Minh, J. Am. Ceram. Soc. 76 (1993) 563.
[2] H.L. Tuller, A.S. Nowick, J. Electrochem. Soc. 122 (1975) 255.
[3] T. Inoue, T. Setoguchi, K. Eguchi, H. Arai, Solid State Ionics 35 (1989) 285.
[4] A.V. Virkar, J. Electrochem. Soc. 138 (1991) 1481.
[5] Y. Mishima, H. Mitsuyasu, M. Ohtaki, K. Eguchi, J. Electrochem. Soc. 145 (1998) 1004.
[6] R. Chockalingam, V. Amarakoon, H. Giesche, J. Eur. Ceram. Soc. 28 (2008) 959.
[7] J.S. Lee, K.H. Choi, B.K. Ryu, B.C. Shin, I.S. Kim, Ceram. Int. 30 (2004) 807.
[8] H.J. Park, G.M. Choi, Solid State Ionics 178 (2008) 1746.
[9] W.H. Sutton, Am. Ceram. Soc. Bull. 68 (2) (1989) 376.
[10] W.H. Sutton, Mater. Res. Symp. Proc. 124 (1988) 287.
[11] J.F. MacDowell, Am. Cer. Soc. Bull. 63 (2) (1984) 282.
[12] H. Fukushima, T. Yamaka, M. Matsui, J. Mater. Res. 5 (2) (1990) 397.
[13] J. Samuels, J.R. Brandon, Mater. Sci. 27 (1992) 3259.
[14] P. Boch, N. Lequeux, P. Piluso, Mater. Res. Symp. Proc. 269 (1992) 211.
[15] S. Al-Assafi, D.E. Clark, Mater. Res. Symp. Proc. 269 (1992) 335.
[16] S. Chockalingam, D.A. Earl, V.W. Amarakoon, Int. J. Appl. Ceram. Technol. 6 (1) (2009) 102.
[17] S. Chockalingam, V.R.W. Amarakoon, J. Ceram. Soc. Jpn. 116 (6) (2008) 700.
[18] S. Chockalingam, J. George, D.A. Earl, V.R.W. Amarakoon, J. Micrrowave Power Electromagn. Energy 42 (2) (2008) 4.
[19] M.A. Janney, C.L. Calhoun, H.D. Kimrey, J. Am. Ceram. Soc. 75 (2) (1992) 341.
[20] Y.P. Fu, S.H. Chen, Ceram. Int. 36 (2) (2010) 483.
[21] L.L. Hench, J.K. West, Chemical Processing of Advanced Materials, John Wiley & Sons, Inc., 1992, p. 288.
[22] K.H. Brosnan, G.L. Messing, D.K. Agrawal, J. Am. Ceram. Soc. 86 (8) (2003) 1307.
[23] Y. Fang, J. Cheng, D.K. Agrawal, Mater. Lett. 58 (2004) 498.
[24] Y.V. Bykov, K.I. Rybakov, V.E. Semenov, J. Phys. D: Appl. Phys. 34 (2001) 55.
[25] A. Birnboim, J.P. Calame, Y. Carmel, J. Appl. Phys. 85 (1999) 478.
[26] J.H. Booske, R.F. Cooper, S.A. Freeman, B. Meng, K.I. Rybakov, V.E. Semenov, Microwaves: Theory and Applications in Materials Processing IV, vol. 80, American Ceramic Society, Westerville, OH, 1997.
[27] B.E. Yoldas, Am. Ceram. Soc. Bull. 54 (3) (1975) 289.
[28] X. Zhang, Z. Xie, L. Xu, W. Yang, Mater. Des. 30 (2009) 4507.
[29] A. Heuer, N. Claussen, W.M. Kriven, M. Ruhle, J. Am. Ceram. Soc. 65 (12) (1982) 642.
[30] J. Mckittrick, B. Tunaboylu, J. Katz, J. Mater. Sci. 29 (1994) 2119.

[31] Q. Feng, S. Chockalingam, D.A. Earl, J. Am. Ceram. Soc. 89 (2006) 3770.
[32] V. Viswanathan, T. Laha, K. Balani, A. Agarwal, S. Seal, Mater. Sci. Eng. R 54 (2006) 121.
[33] D.L. Johnson, in: G.C. Kuczynski, A.E. Miller, G.A. Sargent (Eds.), Sintering and Heterogeneous Catalysis, Plenum Publishing Corp., NY, 1984, p. 243.
[34] H. Li, C. Xia, M. Zhu, Z. Zhou, G. Meng, Acta Mater. 54 (2006) 721.
[35] K. Huang, R.S. Tichy, J.B. Goodenough, J. Am. Ceram. Soc. 81 (10) (1998) 2576.
[36] Y.J. Kang, H.J. Park, G.M. Choi, Solid State Ionics 179 (2008) 1602.
[37] S. Li, Z. Li, B. Bergman, J. Alloys Compd. 492 (2010) 392.
[38] J. Maier, Prog. Solid State Chem. 23 (1995) 171.